Self-Assembly of Block Copolymer Thin Films and Their Applications

Sohyeon Bae

Department of Energy Engineering
(Battery Science and Technology)

Graduate School of UNIST

Self-Assembly of Block Copolymer Thin Films and Their Applications

A thesis
submitted to the Graduate School of UNIST
in partial fulfillment of the
requirements for the degree of
Master of Science

Sohyeon Bae

06. 08. 2017

Approved by

Advisor
Soojin Park

Self-Assembly of Block Copolymer Thin Films and Their Applications

Sohyeon Bae

This certifies that the thesis of Sohyeon Bae is approved.

06. 08. 2017

Signature

Thesis supervisor: Soojin Park

Signature

Jungki Ryu

Signature

Seok Ju Kang

Contents

List of Figures

Abstract

Inorganic nanomaterials have paid much attention in promising research fields because of their unique properties such as quantum effects, surface functionalization, and high surface-to-volume ratio. Furthermore, arrays of nanomaterials like nanodot and nanopattern remarkably improved electronic and optical properties. Among a rich variety of templates for nanomaterials, functional block copolymers (BCPs) are very useful and effective, because metal ions are selectively incorporated into one of the blocks via electrostatic interactions, and morphologies and size can be easily tuned in nanoscale according to their molecular weights of two different blocks. Herein, we demonstrate the synthesis of highly ordered inorganic nanomaterials by using poly(styrene-block-4-vinylpyridine) and poly (styrene-block-acrylic acid) copolymer templates. The resulting arrays of inorganic nanomaterials are applied to various applications including energy conversion devices and chemical sensors

Chapter 1. Block copolymer self- assembly

1.1. Introduction

1.1.1. Basic Principle of Block Copolymer Self Assembly and Their Applications

The self-assembly of amphiphilic molecules have various morphologies such as spheres, cylinders, lamellae and vesicles. The morphologies are determined by critical packing parameter (γ), $\gamma = v/a_0 l_c$, where v is molecular volume, a_0 is the optimum head group area, and l_c is effective maximum chain extension. Figure 1.1 shows the preferred geometries based on the value of γ, when critical packing parameter, $\gamma < 1/3$, form spheres, $1/3 < \gamma < 1/2$ form cylinders, and $1/2 < \gamma < 1$ form flexible lamella or vesicles. Finally, planar lamellas are formed, when $\gamma = 1$.[1] This theory works well in characterizing simple aggregated shapes such as spheres and cylinders.[2]

Also, copolymers appear similar self-assembly tendency based on packing parameter (p), Especially, copolymer aggregates indicate higher stability and durability than small molecule aggregates because of their mechanical and physical properties.[3-6] Among various copolymers, the block copolymer (BCP), two or more different blocks are connected with covalent bonding, is the most studied field about self-assembly for several decades. Figure 1.2 shows various structures of diblock copolymers with A and B blocks.[7] In general, the diblock copolymers containing A block and B blcok, as shown Figure 1.3. (a), can micro-phase separate into various morphologies including sphere, cylinder, gyroid, lamellae, and etc., in bulk system as shown Figure 1.3(c).[8]

Microphase separation occurs following three key factors, (1) the total degree of polymerization (the number of monomeric units, $N = N_A + N_B$), (2) the polymer volume fraction, (f_A and f_B, the volume occupied by immiscible A and B block, $f_A + f_B = 1$), (3) the Flury – Huggins segment – segment interaction parameter, χ_{AB}, in case of diblock copolymer. The χ_{AB} is temparature dependence, and relationship between χ_{AB} and temparature (T) is shown in eqn (1) : [5,6]

$$\chi_{AB} = \left(\frac{z}{k_B T}\right)\left[\varepsilon_{AB} - \frac{1}{2}(\varepsilon_{AA} + \varepsilon_{BB})\right] \qquad (1)$$

z is the number of neighboring monomers per repeat unit in the polymer, k_B is the Boltzmann constant, and ε_{AB}, ε_{AA}, and ε_{BB} mean interaction energies per repeat unit of A-B, A-A, and B-B. As a result, Figure 1.3(b) indicates theoretical phase diagram of AB diblock copolymers according to χN and f_A. The χN contributes entropy and enthalpy term. Therefore, nanostructure morphologies are determined by balance between entropy and enthalpy term to minimize total free energy in equilibrium condition as a function of the volume fraction of copolymer. [3,6,9]

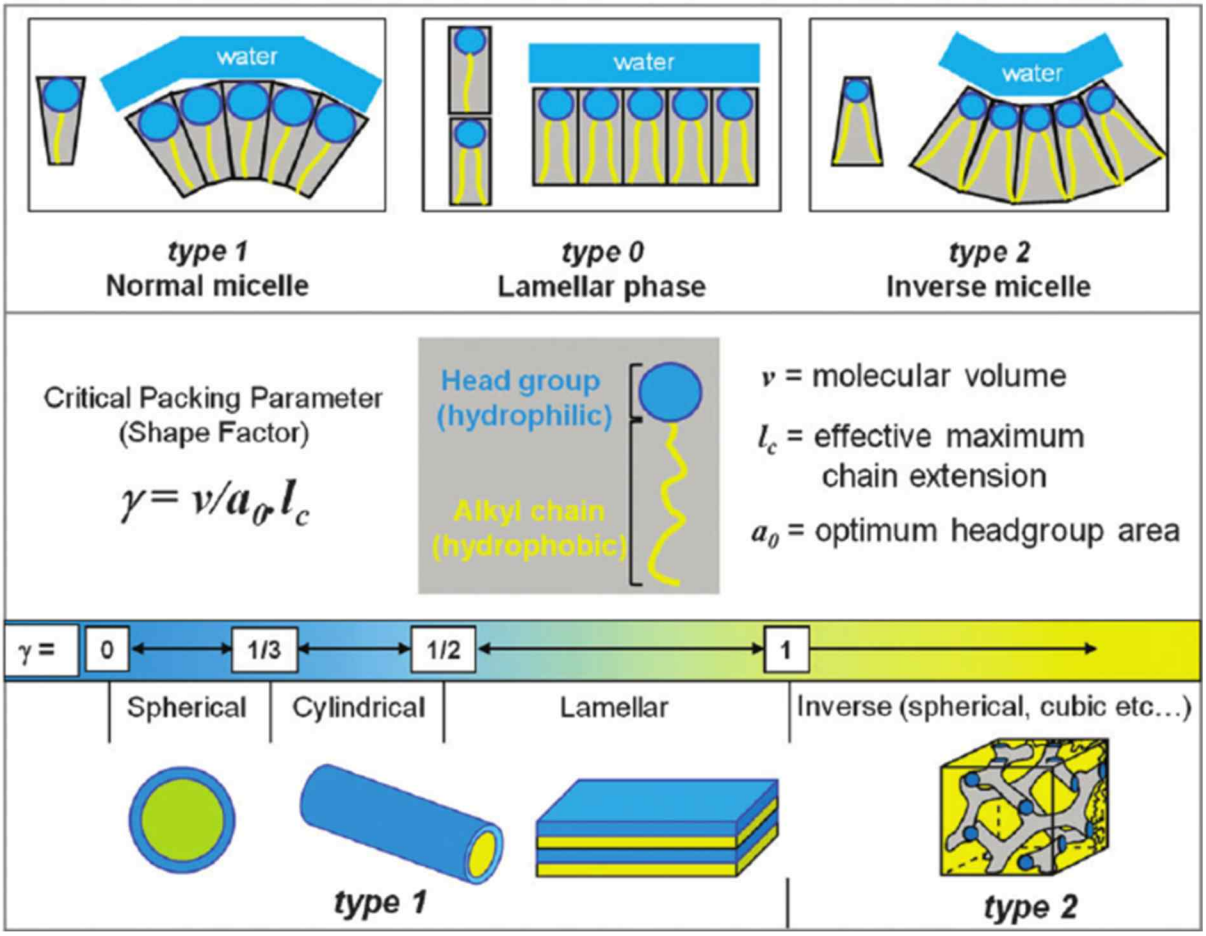

Figure 1.1. Molecular shape and type of amphiphilic self-assemblies. Depending on the critical packing parameter of an amphiphilic molecules, different shape micelles are formed.[1]

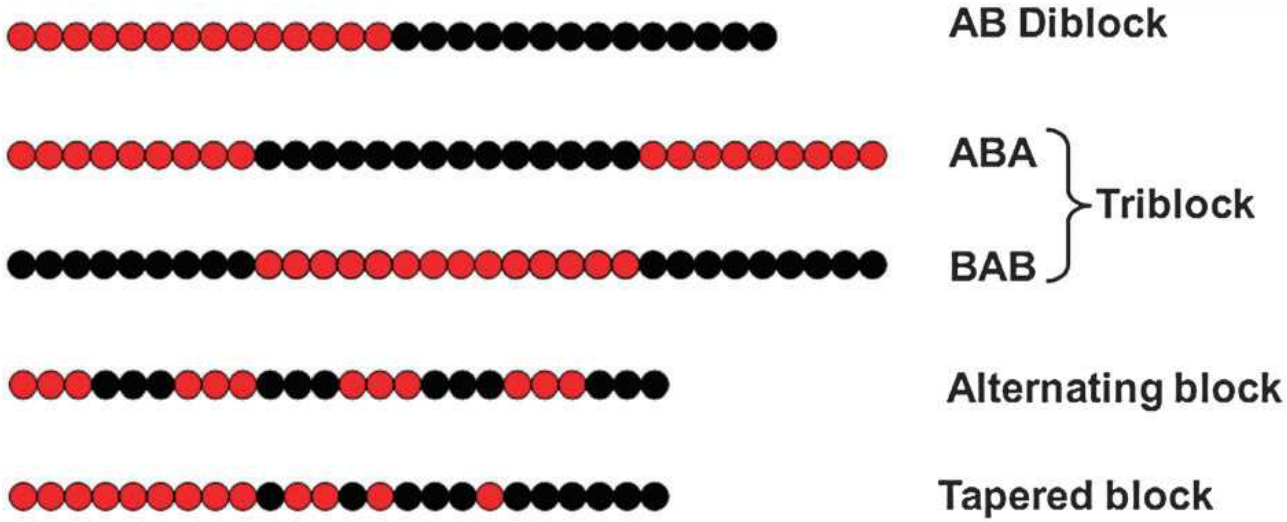

Figure 1.2 Schematic illustration of various block copolymer structures typically containing two types of blocks, A and B.[7]

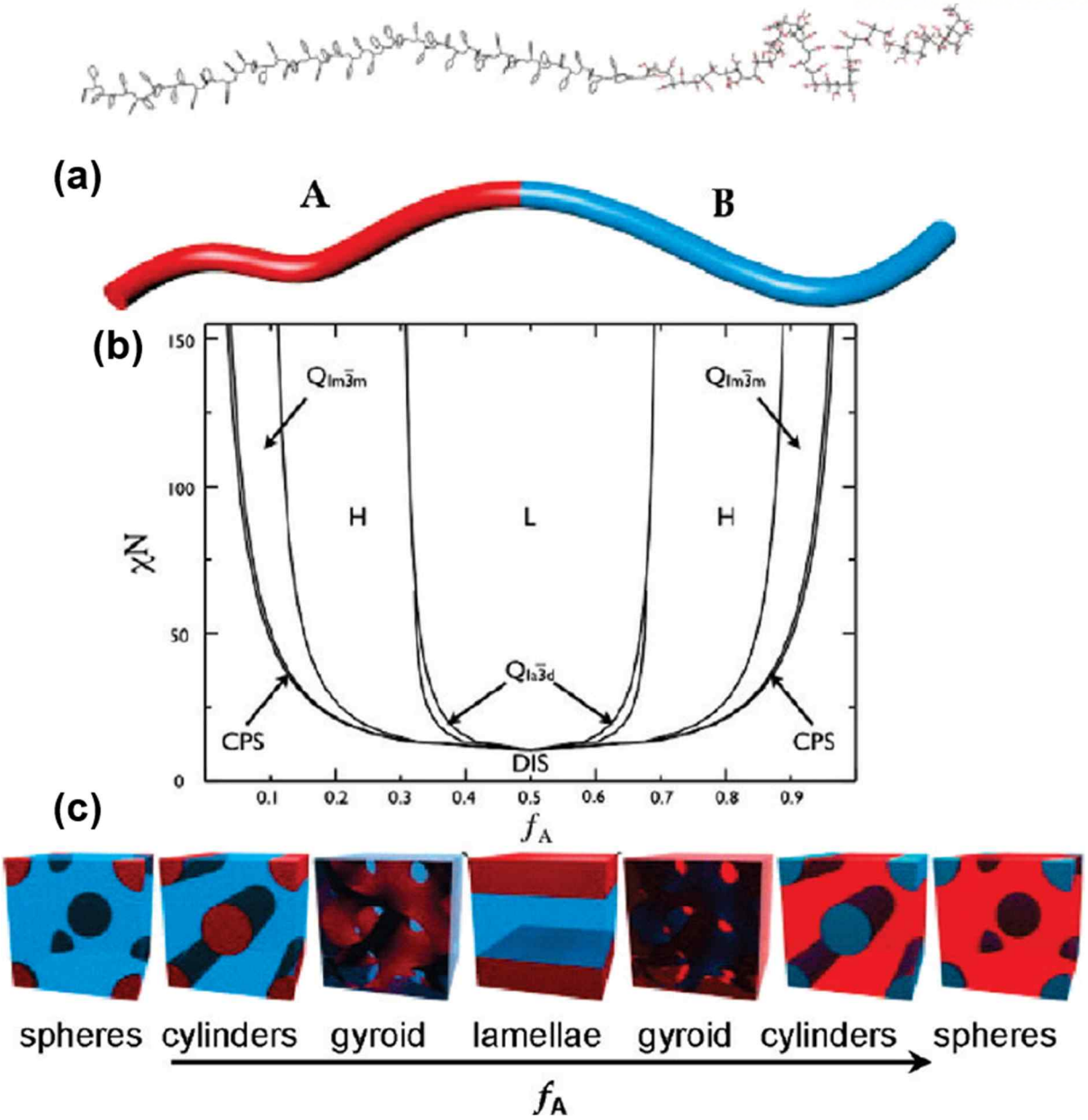

Figure 1.3. (a) Schematic illustration of AB diblock copolymer, (b) diblock copolymer of a mean-field phase diagram, and (c) their six morphologies. Phases are labeled as follows: S (spheres), C (cylinders), Q_{la3d} (gyroid), L (lamellar), Q_{Im3m} (body centered cubic spheres), CPS (close-packed spheres), and DIS (disordered).[27]

1.1.2. Major factor affecting the aggregates in solvent system

In common with amphiphilic molecules, amphiphilic block copolymers are determined by packing parameter, $p = v/a_0 l_c$, where a_0 is the contact area of the head group, l_c is length of hydrophobic segment, and v is volume of hydrophobic block. Figure 1.4. indicates various self-assembled micelle structures according to packing parameter. When $p < 1/3$, form spheres, $1/3 < p < 1/2$ form cylinders, and $1/2 < p < 1$ form flexible lamella or vesicles. Finally, planar lamellas are formed, when $p = 1$.[10]

As mentioned in previous chapter, the abilities of morphology change are determined by free energy in the block copolymer systems.[11,12] Especially, the amphiphilic block copolymers, which have one hydrophobic block and another hydrophilic block, have contrasting affinities for an aqueous solvent. Therefore, amphiphilic block copolymers are aggregated themselves so that the hydrophobic blocks are minimized from the aqueous for a minimum free energy state. And then, as the concentration of amphiphile in solution is increased, the free energy of the system begins to rise due to unfavorable interactions between aqueous solvent and the hydrophobic region of the amphiphile. Consequently, the structure of block copolymers in aqueous system changes to a morphology in which entropy decreases. On the other hand, it takes place in the same way between the hydrophobic solvent and the hydrophilic region of the amphiphilic group. Therefore, the block copolymer aggregates in solvent system are determined by follow key parameters, the degree of stretching of the core-forming blocks (an entropic contribution), the interfacial tension between the micelle core and the solvent outside the core, and the repulsive interactions among corona-forming chains (an enthalpic contribution).[11,12] And then, these three parameters can be contributed by copolymer composition and concentration[13], solvent composition and concentration,[14,15] and additives.[16]

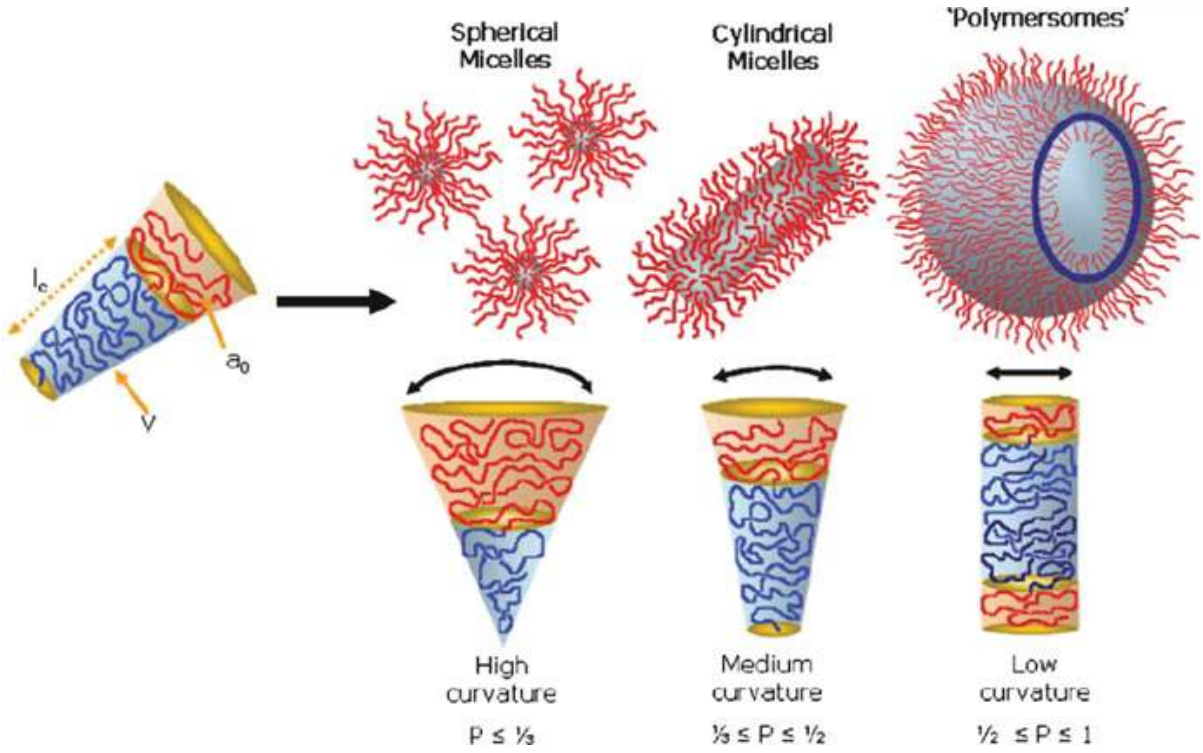

Figure 1.4. Schematic illustration of various micelle structures formed by self-assembled amphiphilic block copolymer in the selective solvent.[10]

1.1.3. Block copolymer nanolithography for nano-template.

Nanoparticles are 1 to 100nm size of particles and have unique electrical, optical, and magnetic properties that are different from conventional bulk particles. Because nanoparticles have high surface to volume ratio and surface energy, they exhibit the activated surface, low melting point and sintering at low temperatures comparing with bulk. Based on these unique properties, nanoparticles have been studied on various applications such as light emitting diode, sensor, bio, and catalyst for the past several years.[17]

There are two types of lithography methods for synthesizing nanoparticles. 'Top-down' and 'bottom-up'. The 'Top-down' approach is that the nanostructure is synthesized by etching away crystal planes on the substrate. Therefore, 'top-down' method, especially photolithography, shows fundamental limitation such as dispersion of light and limitation of light source.[18,19] On the other hand, a 'bottom-up' approach, such as block copolymer lithography, means that the nanostructure is synthesized onto the substrate by stacking atoms, rise to crystal planes, and resulting in the nanostructures.[20] Several methods have been introduced to synthesis arranged metal nanoparticles using block copolymer nano-template. Pinnavaia group firstly utilized self-assembled block copolymers as inorganic material nano-template in 1995. They used the low-molecular-weight block copolymer as template, and Si ions were loaded on the template.[21] Consequently, well-ordered porous silica was obtained. After that, many researchers studied about block copolymer nanolithography using high-weight block copolymers. In this paper, I introduce two types of block copolymer nanolithography using sol-gel method. The first method is that metal ions are directly capped with selective block in solution system.[22] Second method is that metal ions are loaded on prepared block copolymer thin film template.[23] And, the morphology of block copolymer can be controlled through annealing process.[24]

1.1.4. Synthesis of arranged inorganic nanoparticles using block copolymer nano-template

Generally, sol-gel method involves three steps, as illustrated in figure 1.5. Firstly, block copolymers occur micro-phase separation, which separate the block copolymers into hydrophilic and hydrophobic domains in a solvent. And then, the inorganic precursors cooperate with the selective block in self-assembled block copolymers. Secondly, the formation of an inorganic network caused by condensation reactions of the inorganic precursors. These reactions can be tuned to take place simultaneously or subsequently as the self-organization proceeds. Finally, the block copolymer template can be eliminated by calcination or solvent extraction. In this step, crystalline metal oxides may form during calcination, depending on the applied temperature.[22] Another method is that a self-assembled block copolymer thin film has prepared in advance as nano-template. And then, a metal ions are loaded on a selective block of block copolymer thin film. Before loading the metal ions, the patterns of block copolymer thin film are changed by annealing process.[23,24]

1.1.5. Annealing system.

The block copolymer thin films are determined by a degree of confinement within film thickness comparable to the polymer domain spacing. The confined polymers are unfavorable to stretch out or compress their chains. As a result, the self-assembled block copolymers relieve the stretching or compression, and relax the entropic penalty with favorable enthalpic interactions at the substrate or free surface. Two major categories of confinement are defined for substrate-supported block copolymer thin films: "hard" confinement and "soft" confinement. "hard" confinement describes a polymer film confined between two rigid interfaces and "soft" confinement describe a polymer film confined between substrate and the atmosphere.[25] Therefore, in case of a block copolymer thin film confined to the substrate/polymer ("hard" confinement) and air/polymer interface ("soft" confinement), the selective affinity of one block to the substrate or air-interface generates a parallel orientation of cylindrical micro-domains or lamellar micro-domains, or the preferential interaction of the substrate with one block. However, the perpendicular structures are preferred than the parallel structure for applications of block copolymer nano-templates. For this reason, many studies have been conducted for the orientation of micro-domain arrays developed through modification of the surface characteristics and the application of external fields.[24]

Here are two ways to modify surface morphology through solvent vapor and thermal annealing. The synthesis process of fingerprint pattern of Pt lines on substrate is described in Figure. 1.6. (b) as follows: (1) The PS-b-P2VP block copolymer, a molecular weight of PS(32500)-b-P2VP(12000), create micelles structure in a toluene solvent; (2) The PS-b-P2VP solution spin-coat on a Si/SiO_x; (3) Fingerprint pattern of P2VP cylinders in PS matrix is obtained by thermal annealing at 230°C, above the glass transition temperature of both polymer blocks; (4) When the monolayer of PS-b-P2VP cylinder is immersed into a 10mM $Na_2[PtCl_4](aq)$ solution for 24h; (5) After 30s oxygen plasma exposure, Pt ion is reduced to Pt(0) and polymer layer is removed.[23] In addition to thermal-annealing of block copolymer above T_g, solvent vapor annealing (SVA) also cause morphology change. The solvent molecules influence on block copolymer mobility and significantly improve lateral ordering of the block copolymer microdomains. Both, the concentration of block copolymer and the type of solvent importantly affect obtaining film with well-ordered microdomains. The amount of swelling of the block copolymer thin film depends on the chemical nature of the blocks, the quality of the solvent, and the molecular weight of the block copolymer during SVA system. A high degree of swelling provides a high chain mobility, and results in the formation of arrays of ordered microdomains with large grain sizes after SVA in neutral solvents. And then, the removal of solvent causes the degradation of order due to the confinement of block copolymer thin film. Figure. 1.7. shows different micro-domain arrangement due to solvent vapor and thermal annealing.[24] In this study, polystyrene-*b*-poly(methyl methacrylate) (PS-b-PMMA) thin film was used as a neutral substrate. During solvent annealing process, the block

copolymer film shows a generally parallel orientation of the cylindrical PS microdomains over the underlying perpendicular PS cylinders on the substrate because the PMMA is selective blocks for acetone vapor. Continuously, thermal annealing is conducted for structure reorganization to an equilibrium morphology with the perpendicular arrangement of the lamellar microdomains.

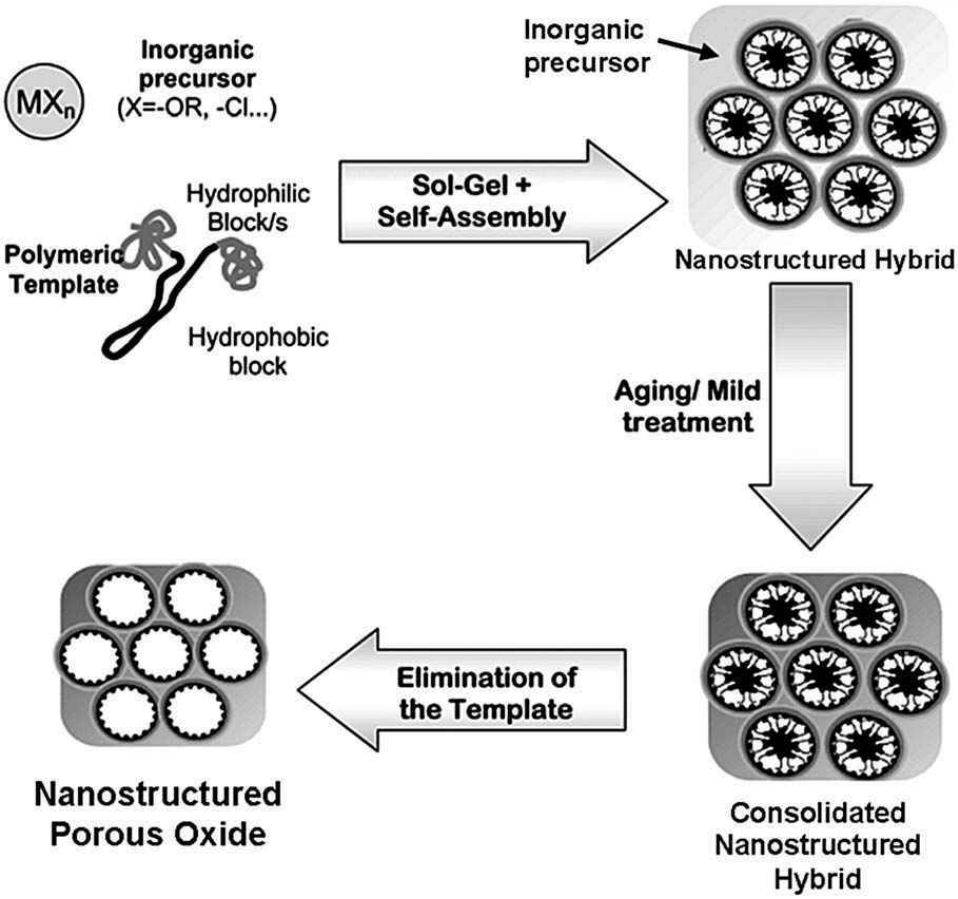

Figure 1.5 The synthesis method of nanostructured porous oxide using self-assembled amphiphilic block copolymer in the solvent.[22]

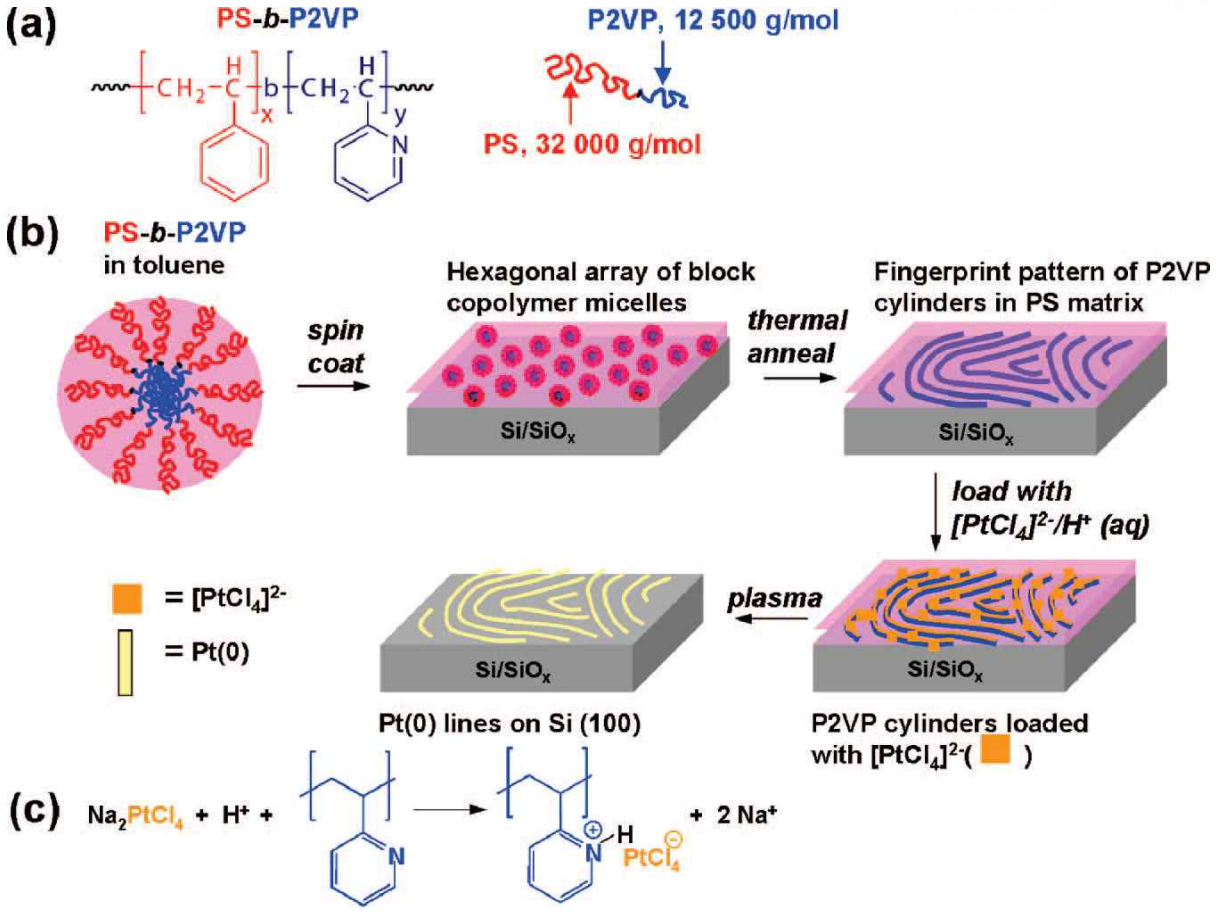

Figure 1.6. (a) Illustration of the PS-b-P2VP block copolymer. (b) Fabrication process of Pt(0) lines coated on Si (100). (c) Cooperation of P2VP block with anionic metal ions in an acidic environment.[23]

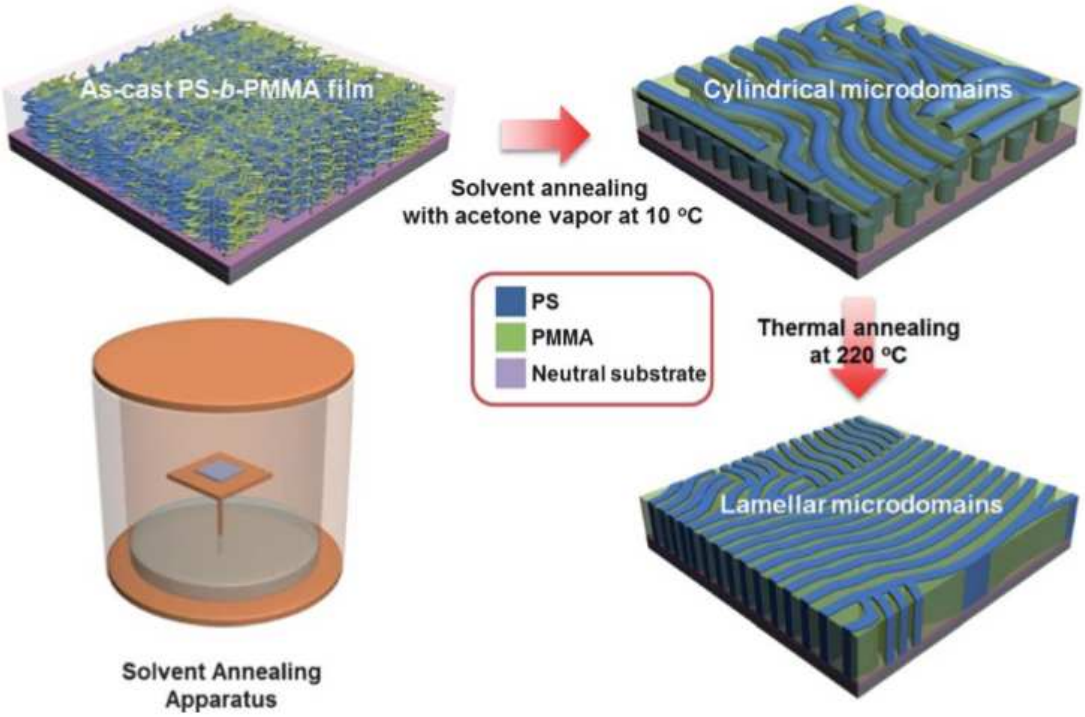

Figure 1.7. Sequential process for PS-b-PMMA films by solvent annealing with acetone vapor and thermal annealing.[24]

As various application fields using nanostructures are increasing, block copolymer self-assembly is attracting attention for the nanolithography. Because block copolymer nanolithography is required to relatively low cost and simple manufacturing process comparing with photolithography process. The photolithography process, generally used as top-down method, shows fundamental restrictions such as dispersion of light and limitation of light source. On the other hand, block copolymer self-assembly, the micro-phase separation of block copolymer, forms a uniform nanostructure without additional complicated manufacturing processes. And, it has been studied in bulk, solution state, and thin film state. Especially, thin film systems can further arrange to well-ordered morphology due to annealing process. Therefore, nanocomposite of block copolymers is used for various application such as template, scaffold, cell culture substrate, separator and anti-reflection coating for synthesis of catalyst, organic and inorganic structures.

In this section, we demonstrated the desired template by adjusting the molecular weight block copolymers. Therefore, we can control the various size and spacing of inorganic nano-template. In addition, we observed that the micelle morphology can easily change through solvent vapor annealing process. Finally, we loaded Ag, Au, and metal oxide nanoparticles on the template. Accordingly, we confirmed that block copolymer nano-template is suitable for nano-lithography of inorganic materials.

1.2. Experimental section

1.2.1 Block copolymer solution and thin film

1wt% of polystyrene-block-poly(2-vinylpyridine) (PS-*b*-P2VP) copolymer was dissolved in toluene at 70 °C with stirring for 4 h. Toluene is a good solvent for PS block and non-solvent for P2VP block, so that the spherical micelle was formed with a PS(shell)-*b*-P2VP(core) copolymer. The PS-*b*-P2VP micellar film was spin-coated onto Si wafer.

1.2.2 Solvent vapor annealing system

Block copolymer thin film coated Si wafer was put into jar with volume of 250 mL. And then, 0.5 mL of chloroform was injected into the jar to anneal the sample with chloroform vapor. After annealing for proper minutes, block copolymer coated Si wafer was taken out from the jar.

1.2.3 Block copolymer inorganic nano-template

Sol-gel method: Metal precursor was added into block copolymer solution (molar ratio of metal precursor/pyridine=1), and solution was stirred for a day at room temperature. In order to eliminate the residue, metal precursor added solution was filtered using 450 nm syringe filter. After that, the hydrazine solution was dropped for reducing the metal ion, and stirred. The solution was filtered again using a 450 nm syringe filter to remove the reduced metal nanoparticles outside the block copolymer micelle.

Finally, metal ion such as Ti, Fe, Ag, and Au loaded block copolymer solution was spin-coated onto Si substrate and treated with O_2 plasma for 10min to form metal oxides and remove the block copolymer templates. Further, a desired phase of the metal oxide nanoparticles was obtained by performing heat treatment at a specific temperature.

Nano-template: The PS-*b*-P2VP micelle thin films were spin-coated onto substrate at 2000 rpm for 60 s. The PS-*b*-P2VP micellar films were immersed in ethanol for reconstructing to surface modify the film. 0.5 wt% of metal precursor solutions were prepared in ethanol. The block copolymer thin film was immersed in metal precursor solution for a sufficient time to load the metal ion into pyridine group of the specific block P4VP or P2VP. After that, the remaining solution was rinsed with ethanol, and thin film was treated with O_2 plasma or H_2 plasma according to the purpose.

1.3. Result & Discussion

The PS-*b*-P4VP block copolymer dissolved in toluene at 1wt% was spin-coated on the Si substrate to prepare an inorganic nano-template using self-assembled block copolymer micelle. The three different molar weights of block copolymer solutions were prepared, 53.5 $kg \cdot mol^{-1}$ of PS(37.5K)-b-P4VP(16K), 76 $kg \cdot mol^{-1}$ PS(57.5K)-b-P4VP(18.5K), and 136 $kg \cdot mol^{-1}$ PS(109K)-b-P4VP(27K), and block copolymer micelles form different sizes and spacing. As the molecular weight increases, the size of micelles and the distance between micelles also increase. And then, various metal precursors can be loaded with specific site of the cores in block copolymer micelles such as pyridine group of P4VP block copolymer with polar-polar interaction. And its size and spacing can be controllable depending on amount of precursors and molecular weight of block copolymer.

The Figure.1.8 shows scanning electron microscope (SEM) images of uniformly arranged titanium oxide nanoparticles using block copolymer self-assembly. The titanium tetraisopropoxide (TTIP) was added in block copolymer solution (molar ratio of Titanium ion/Pyridine = 1) and stirred for a sufficient time so that the metal precursor was attached to the block copolymer. Titanium-loaded block copolymer thin films were prepared on the Si substrate by spin-coating. And then, thin films were treated with O_2 plasma to oxidize titanium to titanium oxide. In some cases, heat treatment was performed at a desired temperature to increase the crystallinity of the titanium oxide. The Figure. 1.8. (a) shows SEM image of arranged titanium oxide nanoparticles of about 20nm using a PS(37.5K)-*b*-P4VP(16K) block copolymer, figure 1.8. (b) shows SEM image of arranged titanium oxide nanoparticles of about 25nm using a PS(57.5K)-*b*-P4VP(18.5K) block copolymer, and figure 1.8. (c) shows SEM image of arranged titanium oxide nanoparticles of about 40nm using a PS(109K)-*b*-P4VP(27K) block copolymer. Consequently, we demonstrate a spherical inorganic nano-template that can control size and spacing

between nanoparticles a simple block copolymer solution.

Not only spherical micelles but also other morphologies can be controlled by solvent vapor annealing. The block copolymer phase separation in thin films was induced by a solvent vapor annealing process in which the mobility of block copolymer was significantly increased in the vapor of a neutral solvent. The solvent vapor annealing process was proceeded with the 0.5mL of chloroform in a jar with volume of 250 mL. The chloroform is the neutral solvent for both blocks. Figure 1.9 shows a series of height mode AFM (atomic force microscopy) images obtained from PS-*b*-P4VP thin films with different solvent-annealing times. Initially, figure 1.9. (a) shows the dimple-like structure after reconstruction process of spherical micelles of block copolymer thin film. When the block copolymer micelle thin films were immersed in ethanol for an appropriate period of time, the P4VP block was selectively solvated in ethanol. On the other hand, the PS blocks remained in its original fixed state. Therefore, after drying, the P4VP blocks were come out and covered the PS surface to make nano-sized pores without changing the original center-to-center distance of the micelles because of their defined molecular weight.[26] Once the block copolymer thin film was exposed to the saturated solvent vapor, the mobility of block copolymer chains was significantly increased and phase separated. Figure 1.9. (b) shows AFM image of vertically oriented cylinders of PS-*b*-P4VP block copolymer with chloroform vapor annealing for 15 min, and figure. 1.9. (c) shows AFM image of revisited vertically oriented cylinders of PS-*b*-P4VP block copolymer with chloroform vapor annealing for 25min, the lateral ordering of P4VP cylindrical micro-domains were significantly enhanced as compared to figure 1.9. (b).

The various morphologies controlled by solvent vapor annealing is demonstrated in figure 1.9. In addition, the S4VP copolymers with P4VP functional groups can play an important role in nanoreactors synthesizing metal nanoparticles because the pyridine groups of P2VP or P4VP blocks can bind strongly to metal ions. Figure 1.8 shows titanium nanoparticles made of a block copolymer thin film, and figure 1.10 demonstrates that a variety of metal ions, such as Ti, Fe, Ag, and Au ions, can be fabricated as metal nanoparticles through block copolymer self-assembly. The silver nitrate was used as Ag precursor, hydrogen tetrachloroaurate trihydrate was used as Au precursor, titanium tetraisopropoxide (TTIP) was used as titanium precursor, and iron nitrate was used as Fe precursor. Figure 1.10. (a) shows iron oxide nanoparticles, (b) Titanium oxide nanoparticles. The 53.5 $kg \cdot mol^{-1}$ of PS(37.5K)-*b*-P4VP(16K) block copolymer was used as scaffold of metal oxide nanoparticles. 1 wt% of PS-b-P4VP was dissolved in toluene, and then iron nitrate or TTIP was added in block copolymer solution (molar ratio of metal ion/pyridine =1). The Fe-PS-b-P4VP solution or Ti-PS-b-P4VP solution was spin-coated on the Si substrate. Finally, O_2 plasma was treated for oxidation of metal ion. Figure 1.10(c) shows Ag nanoparticles, and (d) shows Au nanoparticles. They used 31$kg \cdot mol^{-1}$ of PS(16K)-*b*-P4VP(15K) block copolymer as scaffold of metal nanoparticles. 1wt% of PS-b-P4VP was dissolved in toluene, and then iron $AgNO_3$ or $HAuCl_4 \cdot 3H_2O$ was added in block copolymer solution (molar ratio of metal ion/pyridine

=1). In here, metal ion was reduced using by hydrazine solution. After reducing the metal ions, the Ag-PS-b-P4VP or Au-PS-b-P4VP solution was spin-coated on Si substrate.

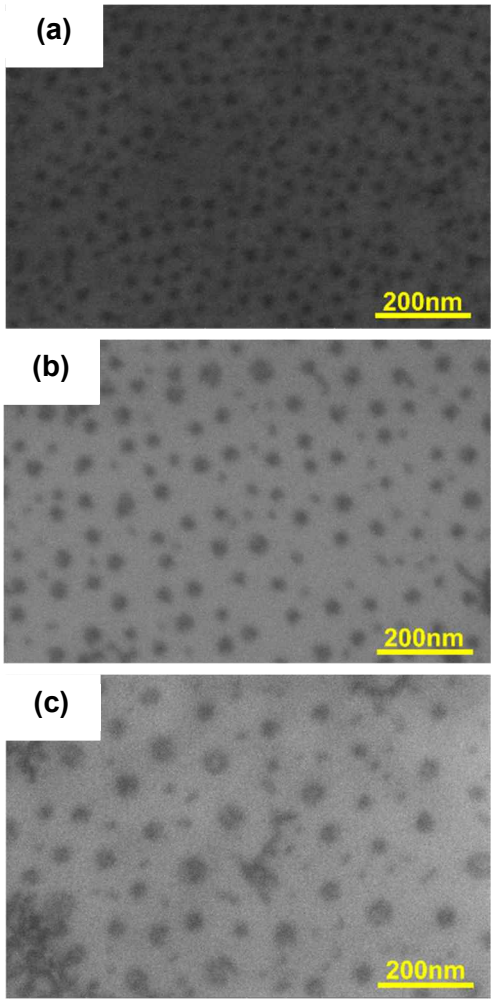

Figure 1.8. (a) SEM image of arranged titanium oxide nanoparticles using PS(37.5K)-*b*-P4VP(16K) block copolymer. (b) SEM image of arranged titanium oxide nanoparticles using PS(57.5K)-*b*-P4VP(18.5K) block copolymer. (c) SEM image of arranged titanium oxide nanoparticles using PS(109K)-*b*-P4VP(27K) block copolymer.

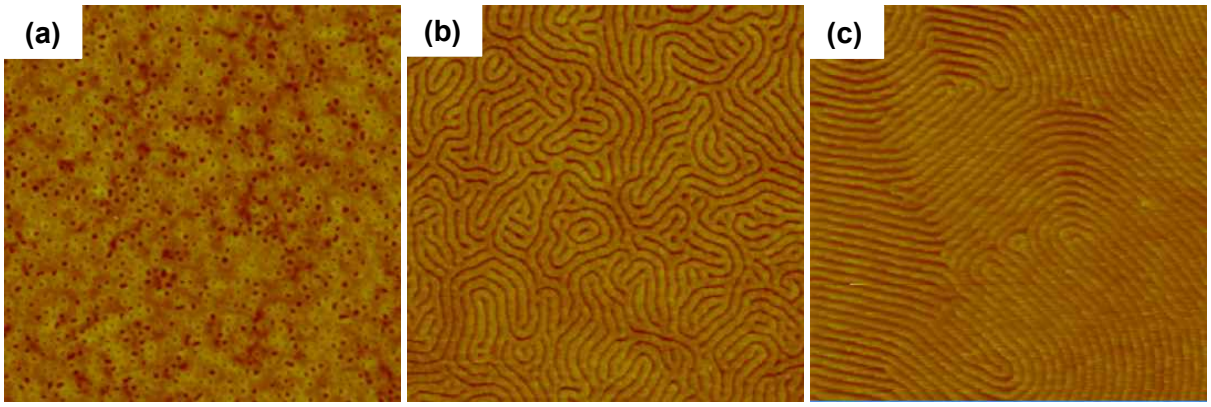

Figure 1.9. AFM images of different morphology at three different exposure time of chloroform vapor: (a) SVA for 0 min, (b) SVA for 15 min, and (c) SVA for 25min in a jar with chloroform vapor.

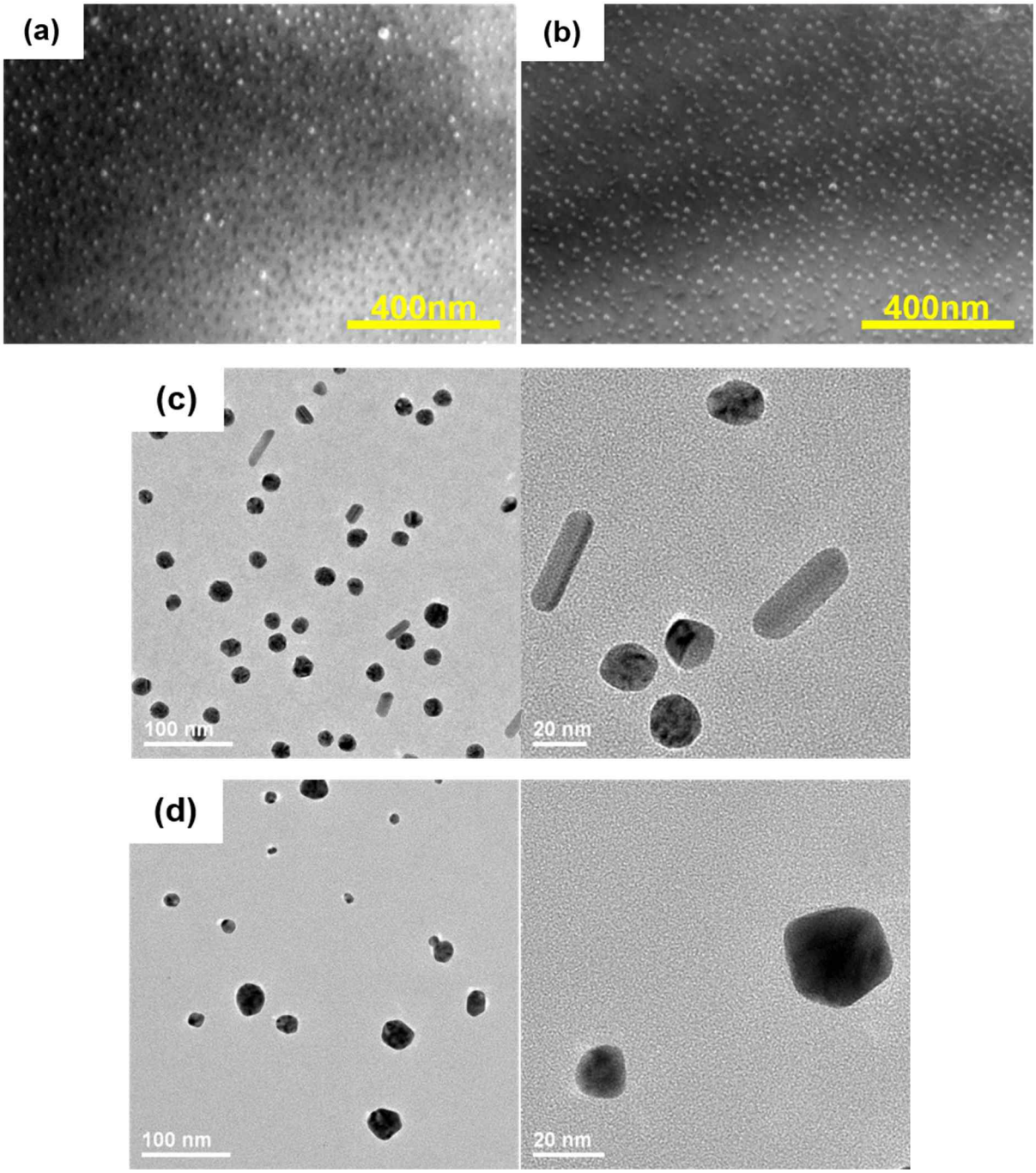

Figure 1.10. SEM images of (a) iron oxide nanoparticles, (b) titanium oxide nanoparticles. (c) Ag nanoparticles, and (d) Au nanoparticles.

1.4. Conclusion

We demonstrated the simple fabrication of block copolymer based inorganic nano-template. We easily controlled the size and spacing between micelles and various morphologies through solvent vapor annealing. In addition, the specific site of the cores in block copolymer micelles, such as pyridine group of P4VP block copolymer, can load the metal ion through polar-polar interaction. Therefore, we indicate a variety of arranged inorganic nanoparticles using self-assembled block copolymer. Through this, it was confirmed that it is suitable for nano-template. This way can be effective way to fabricate various metallic nanostructures. Based on the theories in this chapter, we apply block copolymer self-assembly to energy related application. In the next chapter, I introduce energy related application using block copolymer scaffold, especially about gas sensor application.

References

1. Kulkarni, C. V.; Wachter, W.; Iglesias-Salto, G.; Engelskirchen, S.; Ahualli, S., *Phys. Chem. Chem. Phys.* **2011**, *13*, 3004–3021.
2. Israelachvili, J. N., *Intermolecular and Surface Forces, Elsevier, Amsterdam*, 2011.
3. Alexandridis, P.; Lindman, B., *Amphiphilic Block Copolymers: Self-Assembly and Applications, Elsevier, Amsterdam,* 2000.
4. Thomas, E. L.; Anderson, D. M.; Henkee, C. S.; Hoffman, D., *Nature* **1988**, *334*, 598–601.
5. Bates, F. S., *Science* **1991**, *251*, 898–905.
6. Bates, F. S.; Fredrickson, G. H., *Phys. Today* **1999**, *52*, 32–38.
7. May, Y.; Eisenberg, A., *Chem. Soc. Rev.* **2012**, *41*, 5969–5985.
8. Darling, S. B., *Prog. Polym. Sci.* **2007**, *32*, 1152–1204.
9. Förster, S.; Plantenberg, T., *Angew. Chem. Int. Ed*. **2002**, *41*, 688–714.
10. Blanazs, A.; Armes, S. P.; Ryan, A. J., *Macromol. Rapid Commun*. **2009**, *30*, 267-277.
11. Zhang, L.; Eisenberg, A., *J. Am. Chem. Soc.* **1996**, *118*, 3168–3181.
12. Zhang, L.; Eisenberg, A., *Polym. Adv. Technol.* **1998**, *9*, 677–699.
13. Zhang, L.; Eisenberg, A., *Macromolecules* **1999**, *32*, 2239–2249.
14. Yu, Y.; Zhang, L.; Eisenberg, A., *Macromolecules* **1998**, *31*, 1144–1154.
15. Bhargava, P.; Zheng, J.; Li, P.; Quirk, R. P.; Harris F. W.; Cheng, S. Z. D., *Macromolecules* **2006**, *39*, 4880–4888.
16. Zhang, L.; Eisenberg, A., *Macromolecules* **1996**, *29*, 8805–8815.
17. Whitesides, G. M.; Mathias, J. P.; Seto, C. T., *Science* **1991**, *254*, 1312-1319.
18. Hamley, I. W., *Prog. Polym. Sci*. **2009**, *34*, 1161–1210.
19. Bang, J.; Jeong, U.; Ryu, D. Y.; Russell, T. P.; Hawker, C. J., *Adv. Mater.* **2009**, *21*, 4769–4792.
20. Mingqi Li, Christopher K. Ober, *Materialstoday,* **2006**, *9*, 30-39.
21. Bagshaw, S. A.; Prouzet, E.; Pinnavaia, T. J., *Science* **1995**, *269*, 1242-1244.
22. De G. J.; Soler-Illia, A. A.; Crepaldi, E. L.; Grosso, D.; Sanchez, C., *Curr. Opin. Colloid Interface Sci.* **2003**, *8*, 109-126.
23. Chai, J.; Buriak, J. M., *ACS Nano* **2008**, *2*, 489-501.
24. Gong, J.; Ahn, H.; Kim, E.; Lee H.; Park, S., *Soft Matter* **2012**, *8*, 3570-3575
25. Mai, Y.; Zhang, F.; Feng, X., *Nanoscale* **2014**, *6*, 106 –121.
26. Du, B.; Chen, X.; Zhao, B.; Mei, A.; Wang, Q.; Xu, J.; Fan, Z., *Nanoscale* **2010**, *2*, 1684-1689.
27. Rabotyagova, O. S.; Cebe, P.; Kaplan, D. L., *Biomacromolecules* **2011**, *12*, 269-289.

Chapter 2. Stretchable gas sensor application

2.1. Introduction

Nowadays, electronics have been changed from rigid devices to bendable, rollable, and foldable devices to be applied in wearable devices such as clothes, accessories, and human body. For using as wearable devices, stiff substrate for electronics have to be replaced elastomers and electronic materials have to endure the strain maintaining the conductivity. 2-dimensional materials such as graphene, boron nitride, and metal nanosheets are attractive because they have flexibility because of their unique morphology, which nano-size thickness and bulk dimension.[1] Among them, Au have a ductility that is easily deformed under tensile stress, thus Au nanosheet can relax the condensed force over other 2D materials, and also have outstanding electrical, optical, and mechanical properties.[2] Above all, Au nanosheet is biocompatible, and it shows the potential of bio-devices.

The gas sensor which detect the presence of gases also requires stretchability for various applications. Gas sensor have widely application to gas leakage alarm system, environmental protection, medical diagnosis, military equipment. Recently, the gas explosion accidents happen frequently due to leakage of gases, the importance of gas sensors has been emphasized.[3]

Among various kinds of metal oxide nanomaterials for active material of gas sensor, TiO_2 nanomaterials have been used for various sensor. Because TiO_2 materials are nontoxic, biocompatible, and photo-corrosion free. Furthermore, their inherent properties as nanomaterials, for example, size effect, they can improve the sensitivity of the sensors as compared to general materials.[4,5] Therefore, in this chapter, we tried to improve efficiency of gas sensor by using nano-size TiO_2, and give stretchability to gas sensor by using Au nanosheet with stretchable substrate.

2.1.1. Sensing properties of titanium oxide

TiO_2 have mainly three kinds of phase structure, known as anatase, brookite, and rutile, which band gaps are 3.2, 3.02, and 2.96eV.[6] Anatase and rutile are more stable than brookite, thus they have wider application. Figure 2.1. shows structures of rutile and anatase TiO_2. Rutile TiO_2 has a tetragonal structure and contains 6 atoms per unit cell in which TiO_6 octahedron is slightly distorted. Anatase TiO_2 also has a tetragonal structure, but the distortion of the TiO_6 octahedron is slightly larger for anatase.[7]

The inherent oxygen vacancy in TiO_2 crystal indicates that there is a higher amount of positive charge from Ti than negative charge from oxygen.[8] This type of crystal is enriched in electrons and belong to n-type semiconductors. When the gas is absorbed into the TiO_2 surface, the electrons are released to TiO_2, which increases or decreases the resistance of the TiO_2 materials, a common sensing mechanism for TiO_2-based gas sensors. Furthermore, the conductivity property can be modified by doping metal

elements into TiO_2 materials. And then, by controlling the doping amount and the heating temperature, the n-type TiO_2 materials con be transformed into the p-type.[9]

2.1.2. Synthesis of TiO_2 nanomaterials

TiO_2 nanomaterials can be synthesized by various methods including sol−gel,[10,11] electro deposition,[12,13] micelle,[14] chemical vapor deposition,[15,16] physical vapor deposition,[17,18] direct oxidation,[19] hydrothermal,[20,21] and combined methods[22]. The crystal structures of the TiO_2 materials prepared by these methods are usually rutile or anatase, and sometimes show amorphous state. Certain temperature and pressure are required to create the specific phase structures. It is commonly recognized that nanostructured TiO_2 is more favorable for sensor applications due to their advantages of larger surface area and better electron transition. Figure 2.2. shows TiO_2-based nanostructure with various methods in recent years.[23-26]

2.1.3 Gas sensing mechanism

The gas sensing mechanism can be divided into two types as receptor process and transducer process. Receptor process is conducted by physical absorption by dipole interaction with van der waals, and chemical absorption formed from chemically bonded gas with oxide surface, which interaction between gases and titanium oxide surface. TiO_2 can detect different type of gases both reductive gas (H_2, CO, NH_3, H_2S_3) and oxidative gas (O_2, NO_2), and we can confirm existence of gases through measuring changes in conductivity of the metal oxide. Firstly, when the TiO_2 are exposed to air, oxygen will be absorbed on the TiO_2 surface by forming anionic oxygen. And then, depletion region of TiO_2 will be increase. Therefore, according to doping types (n-doping/p-doping), it causes the change of depletion region and band bending on the surface lead to the alteration of conductivity. For instance, when reducing gases are adsorbed on the anionic oxygen, electrons will be injected from gases into TiO_2 surface, conductivity will be increase by reducing the depletion region and releasing the band bending. On the other hand, when oxidizing gases are adsorbed on the anionic oxygen, electrons transfer TiO_2 surface to adsorbed gases. And then, the conductivity will be decrease by increasing the depletion region as shown figure 2.3(a). Transducer process is transformation of signal occurred from transportation of electrons. This process is performed between grain boundaries, and have an effect due to the electron transfer pattern including surface-controlled, grain controlled, and neck-controlled modes as shown in figure 2.3(b).[27] In the dense layer structure, the gas affects only the geometric surface. Accordingly, the gas sensitivity is determined by the thickness of the thin film like as surface-controlled transducer function. However, the porous structure can affect not only the film thickness but also the pore size and the gas diffusion length of the carrier because the activation site is more than the dense layer structure.[28]

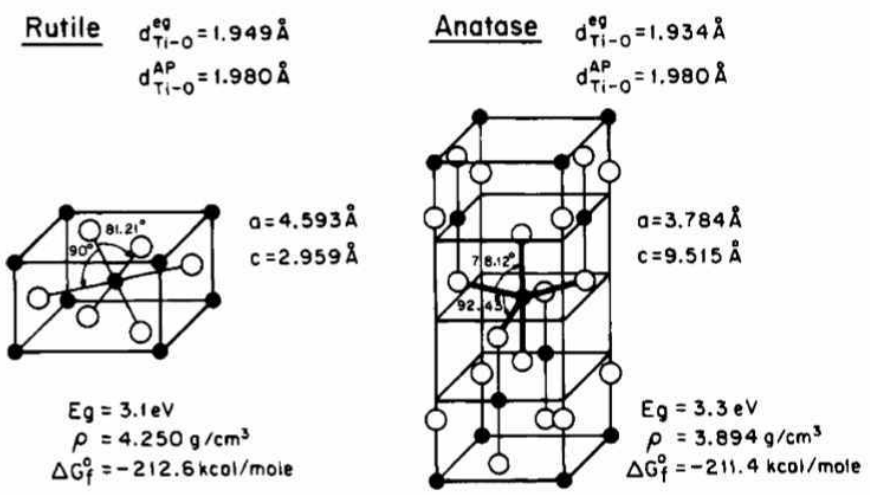

Figure 2.1. Structures of rutile and anatase phase TiO_2.[7]

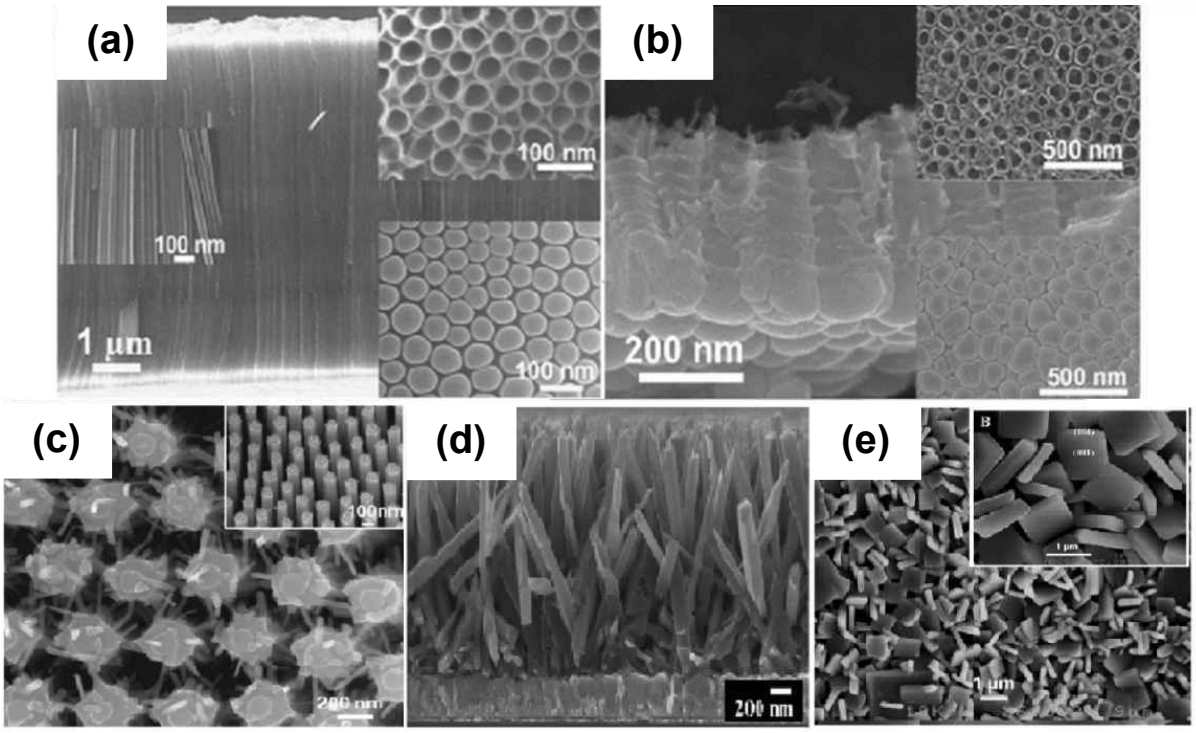

Figure 2.2. (a) Long TiO_2 nanotube arrays from anodization of Ti[23], (b) Short TiO_2 nanotube array from anodization of Ti[23], (c) TiO_2 nanobelts[24], (d) TiO_2 nanorods[25], (e) TiO_2 nanoshets[26].

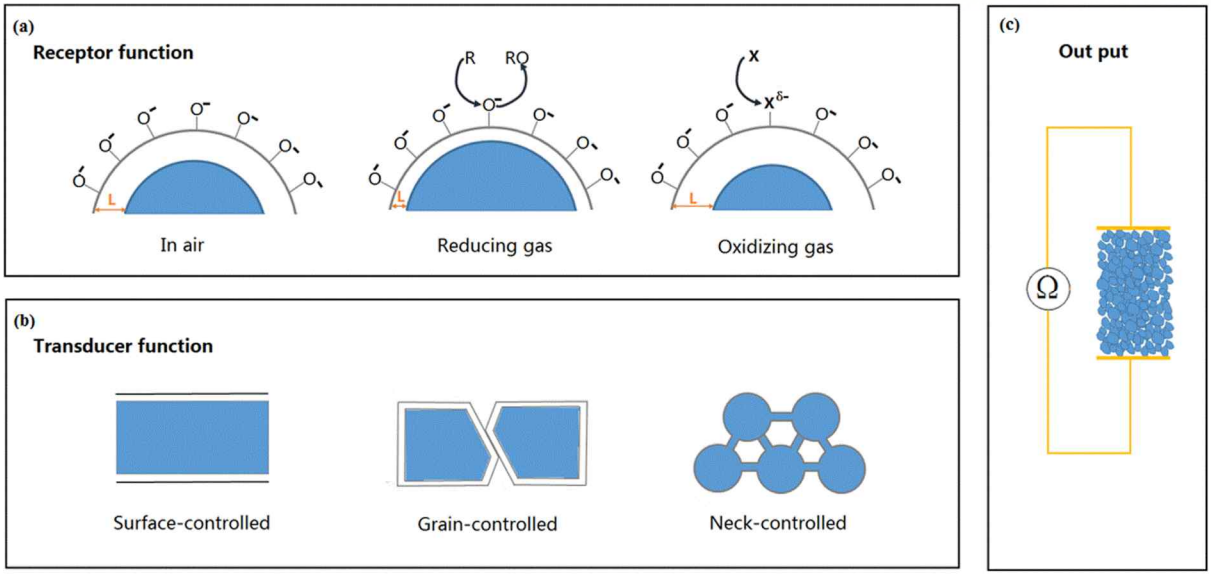

Figure 2.3. Schematic view of gas sensing at different mode. (a) Receptor process, (b) transducer process, and (c) out-put.[28]

2.2. Experimental Section

2.2.1. Fabrication of Au nanosheet substrate

Synthesis of Au nanosheets: 6.8 mg of L-arginine was dissolved in 20mL of D.I water and the solution was heated to 90°C. And, 54mg of hydrogen tetrachloroaurate trihydrate ($HAuCl_4 \cdot 3H_2O$) was dissolved in 8mL of D.I water. And then, solution was rapidly injected heated L-arginine solution for nucleation. The reaction was conducted at 90°C for 2h, after that, cooled down at room temperature. Finally, Au nanosheet was obtained through centrifugation. (Figure 2.4)

Fabrication of Au nanosheet substrate: Firstly, Au nanosheet dispersed in 1-butanol and petri dish filled with D.I. water was prepared. The Au nanosheet solution was dropped on the D.I. water surface using glass pipette. When the monolayer film built on the water surface, Si wafer was put into petri dish and scooped up the Au nanosheet film. (Figure 2.4)

2.2.2. Synthesis of TiO_2 nanoparticles

Synthesis of block copolymer micellar thin film: 1wt% of 53.5kg·mol^{-1} Polystyrene-block-Poly(2-vinylpyridine) (PS-*b*-P2VP) copolymer was dissolved in toluene at 70°C with stirring for 4h. Toluene is a good solvent for PS block and non-solvent for P2VP block, so that a spherical micelle was formed with a PS(shell)-*b*-P2VP(core) copolymer. And then, the PS-*b*-P2VP micelle thin films were spin-coated onto substrate at 2000rpm for 60s.

Fabrication of TiO_2 nanopatterned Au nanosheet for gas sensor: The resulting block copolymer film coated purple wafer was floating on the surface of 1wt% of hydrofluoric acid (HF) aqueous solution, and transferred to deionized (D.I.) water. The floated block copolymer film was transferred onto prepared Au nanosheet coated Si substrate. The PS-*b*-P2VP micellar films were immersed in ethanol for reconstructing the film to modify the film surface, and spherical micellar film was transformed to cylindrical micellar film through solvent vapor annealing process. The solvent vapor annealing process was conducted in 250mL of jar with 0.5mL chloroform solvent for 40min. And then, the sample (Cylindrical micellar block copolymer patterned Au nanosheet coated on Si substrate) was immersed in 1wt% of Titanium precursor solution for loading titanium ions to pyridine group of S4VP copolymer. Finally, O_2 plasma and calcination of sample was treated for oxidation of metal ions. (Figure 2.5)

2.2.3. Fabrication of stretchable gas sensor

The substrate should be changed from rigid substrate to elastomer for stretchable gas sensor. Therefore, we changed Si substrate to polystyrene-b-polybutadiene-b-polystyrene (SBS) block copolymer thin

film. Firstly, we prepared poly(dimethylsiloxane) (PDMS) stamp from ref. 2. The elastomer stamp was made of PDMS by mixing the base monomer and a curing agent (w:w = 10:1) (Sylgard 184, Dow Corning). This PDMS solution was poured into the SU-8 mold and left in air for 2 h to remove air voids. The PDMS stamp was thermally cured at 80°C for 1 day and peeled off of the wafer. Gas sensor material made on Si substrate was stamped with PDMS stamp and transferred onto PDMS stamp. Second, 10wt% of SBS block copolymer solution with chloroform was spin-coated onto the materials transferred PDMS stamp. Finally, after drying chloroform, stretchable gas sensor was obtained.

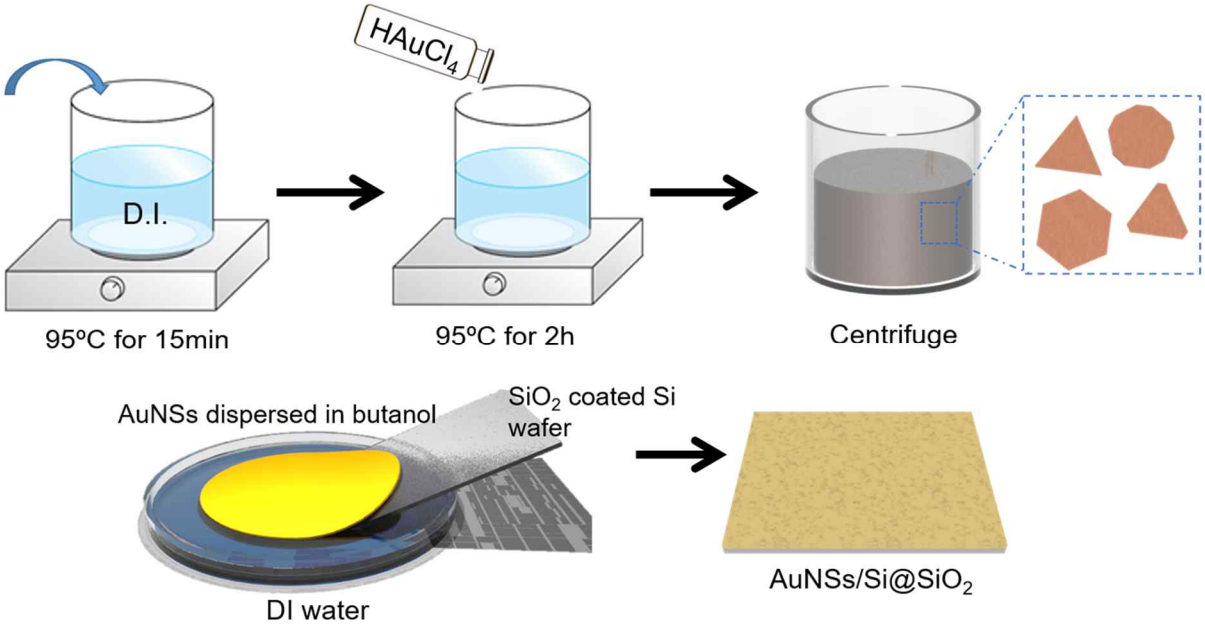

Figure 2.4. Schematic of the synthesis strategies of Au nanosheet.

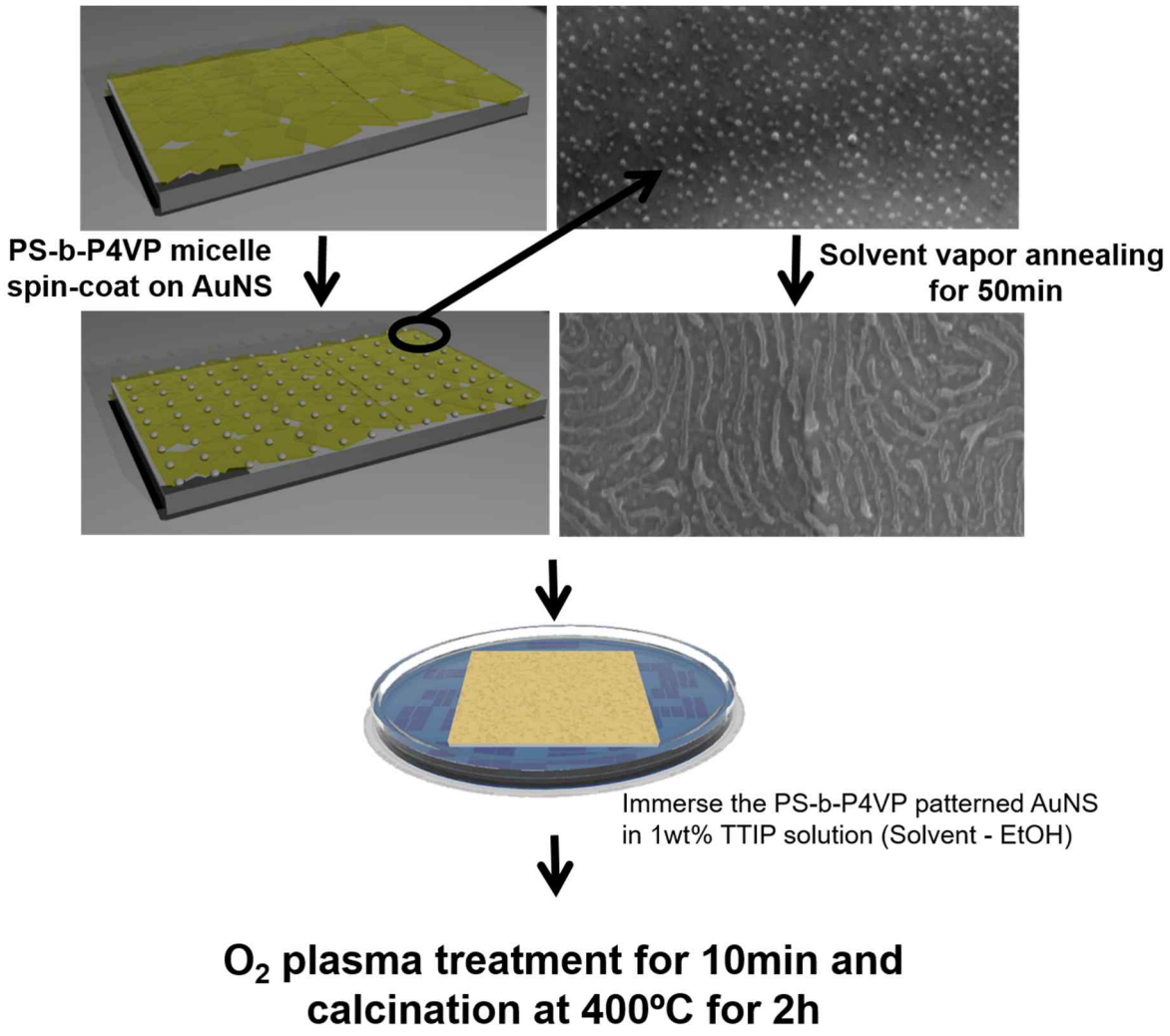

Figure. 2.5. Schematic of synthesis process of TiO_2 nano-patterned Au nanosheets.

2.3. Results and Discussion

2.3.1. Analysis of Au nanosheet

The gas sensor measures the change in the current or resistance due to the detected gas. To this end, the gas sensor requires an active layer that attach the gas and an electrode layer that detects changes in resistance or current. In this chapter, we use Au nanosheets coated SBS thin film as substrate and electrode to give both stretchability and conductivity of sensor. The hydrogen tetrachloroaurate trihydrate ($HAuCl_4 \cdot 3H_2O$) and L-arginine was used as synthetic materials of the Au nanosheet. The L-arginine served as a mild reductant and a capping agent, similar mechanism with the amino acid-based synthesis of Au nanoparticles. Figure 2.6 represents scanning electron microscopy (SEM) images of Au nanosheet. Au nanosheet have a variety of diameter from 15μM to 40μm confirmed by SEM analysis. The unique shape, bulk size and nano-sized thickness of Au nanosheets combine with the ductility of intrinsic property of gold to enhance resistance to internal stresses during stretching. Also, the stacked Au nanosheets can maintain conductivity because they fill each other when stretching. In this paper, Au nanosheet is used only as a stretchable substrate and electrode that maintain conductivity, and the UV-vis spectroscopy confirmed that the absorbance was similar to that of bulk Au rather than Au nanoparticle. The figure 2.7(a) shows UV-vis spectroscopy of Au nanosheets from 300nm to 1400nm. For characterization of the synthesized Au nanosheets, XRD analysis was conducted using Au nanosheets coated with Si wafer. As shown in figure 2.7. (b), in the XRD pattern of the synthesized Au nanosheets, the obtained Au nanosheets are mainly dominated by (111) facets.

2.3.2. TiO_2 patterned Au nanosheet stretchable gas sensor and their gas sensing performance.

There are various TiO_2 nanoparticles synthesis methods such as sol−gel, electrodeposition, micelle, chemical vapor deposition, physical vapor deposition, direct oxidation, hydrothermal, and combined methods. However, it is difficult to synthesize uniform nanoparticles and uniformly arrange nanoparticles after synthesizing them. On the other hand, the block copolymer self-assembled nano-templates can easily synthesize nanoparticles and can be used to increase the efficiency of nanoparticle-based devices by allowing nanoparticles of the desired inorganic material to be arranged in a uniform size. Figure 2.8(a) and (b) show SEM images of a TiO_2 nano-patterned on the Au nanosheet with uniform spacing and size. The size of Au nanosheet was about 20μm. Figure 2.8. (c), (d) represent AFM images of a TiO_2 nano-patterned on the Au nanosheet. The shaded area shown in the Figure 2.8(c) is indicated by the height difference of the Au nanosheets. We confirmed that uniformly nano-patterned and well coated TiO_2 was present on Au nanosheets through SEM and AFM analysis. Finally, we also confirmed that the conductivity is maintained as an electrode when TiO_2 nano-patterned Au nanosheet is folded for use as a stretchable gas sensor. Figure 2.8(e) indicates that the sample maintain a

conductivity of about 10 even if sample is folded. Therefore, it can be used as a gas sensor electrode.

Since we have confirmed that it is used as an electrode, so we have confirmed that it has sensitivity to selective gas. Herein, we used NH_3 as the detecting gas. The H_2, CO, NH_3, and H_2S gases are reducing gases, and when reducing gas is adsorbed on the surface anionic oxygen, electrons will be injected into TiO_2 surface, which will reduce the depletion region and release the band bending; hence, the film conductivity will be improved. The result was obtained with a detection of 2000 ppm NH_3 at room temperature. (Figure 2.9). As the gas injection was turned on and off, the change in current was observed.

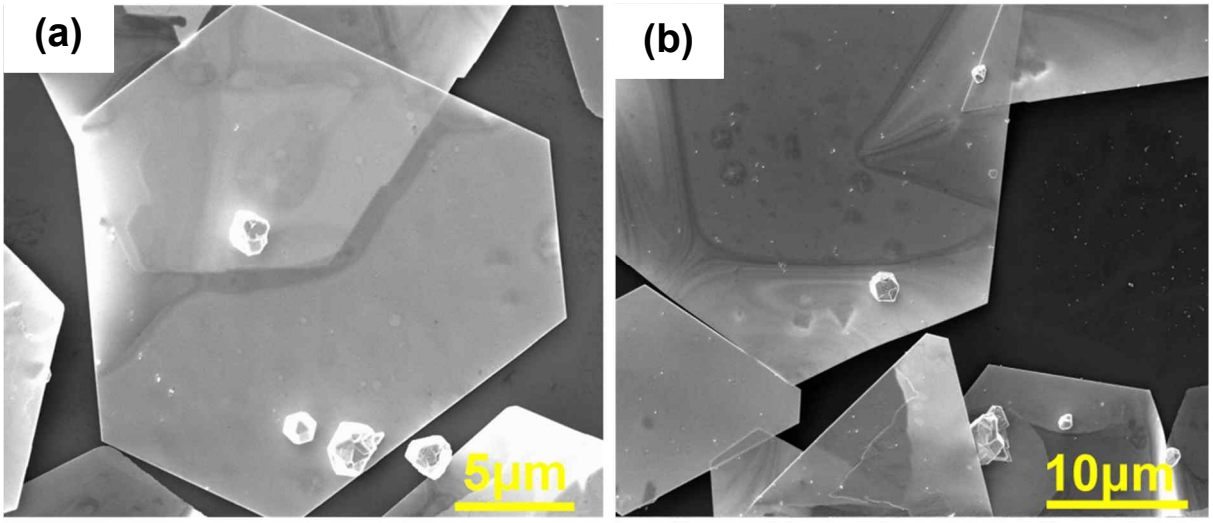

Figure 2.6. Characterization of Au nanosheet. (a, b) SEM images of Au nanosheet at different scales.

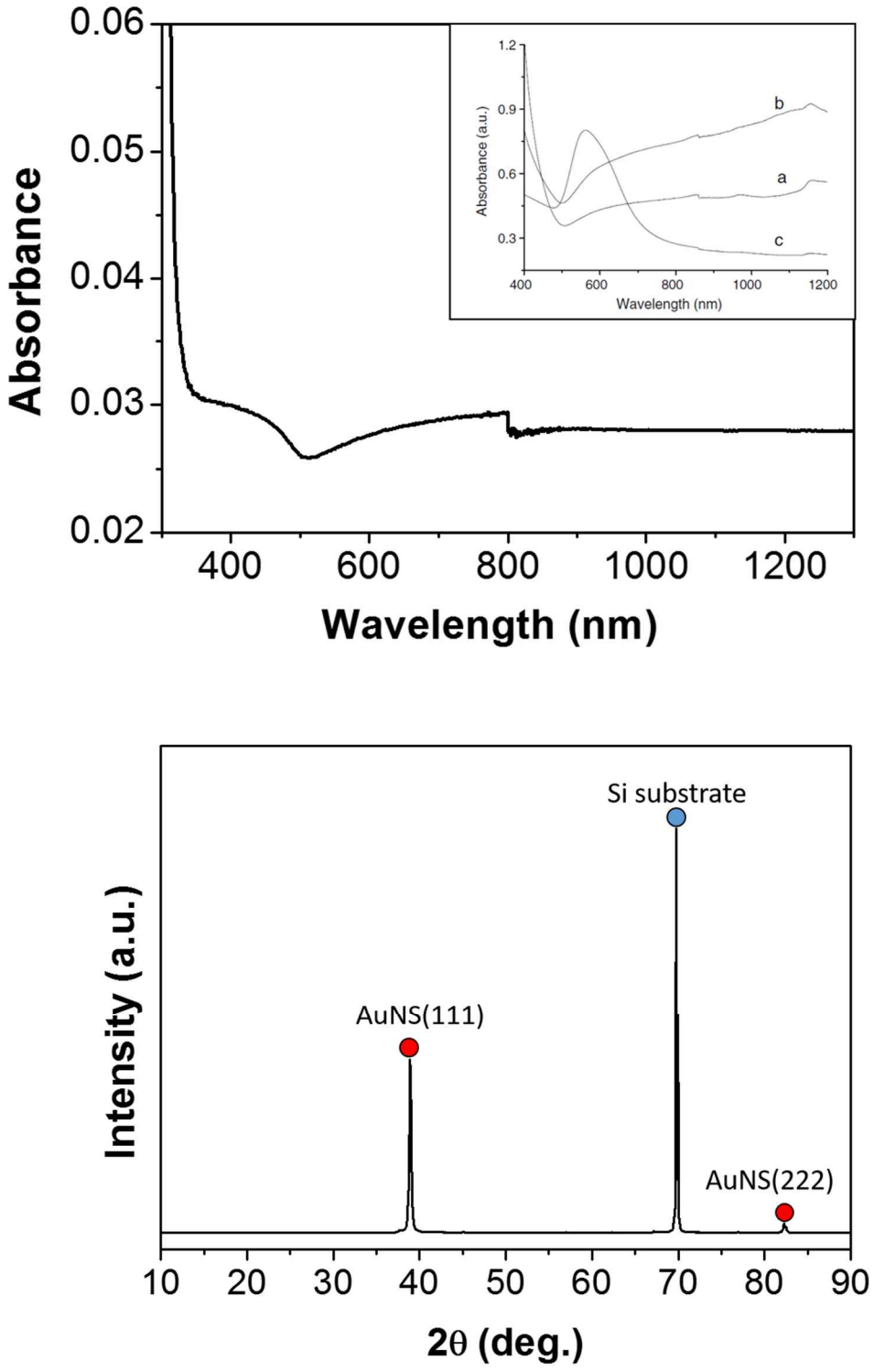

Figure 2.7. Characterization of Au nanosheet. (a) UV-vis spectroscopy of Au nanosheet. (b) XRD pattern of Au nanosheet.

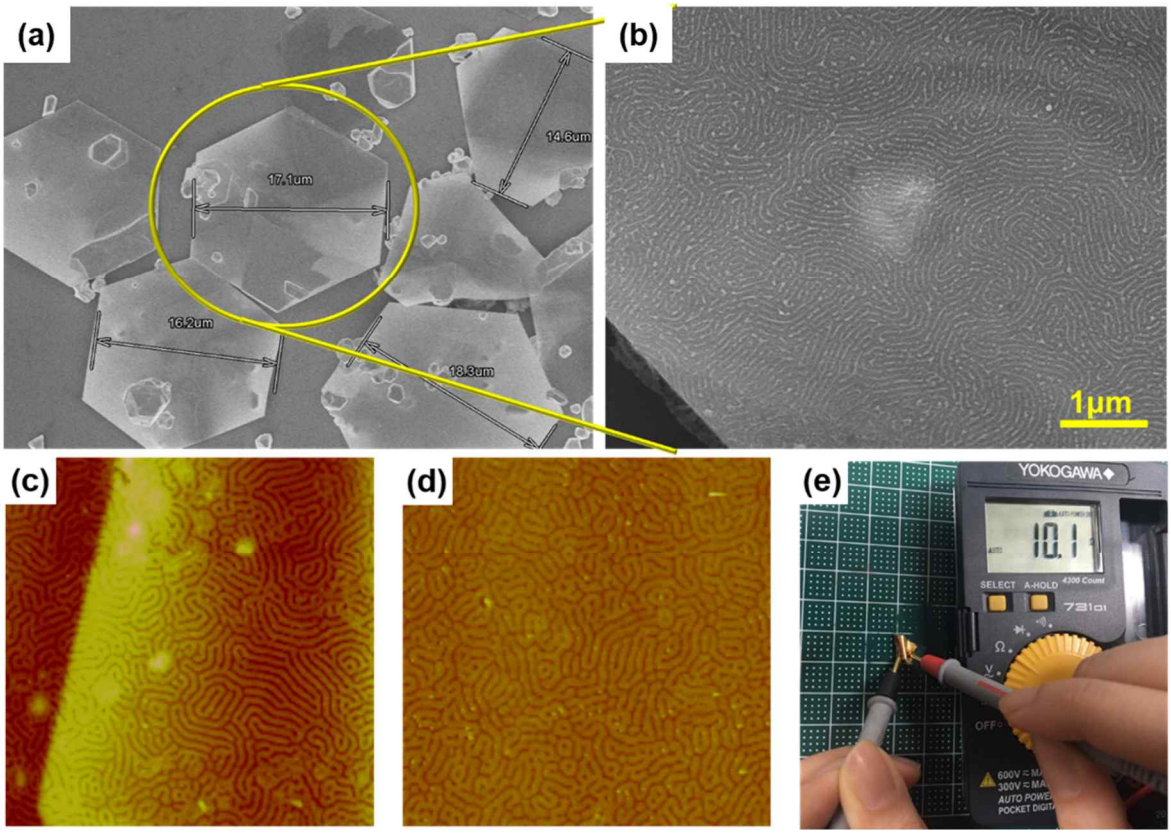

Figure 2.8. SEM images of TiO_2 nano-patterned Au nanosheets (a) Au nanosheets, (b) line patterned TiO_2, and AFM images of TiO_2 nano-patterned Au nanosheets (c), (d) line patterned TiO_2 on Au nanosheets, and (e) photograph of TiO_2 nano-patterned Au nanosheets on stretchable substrate.

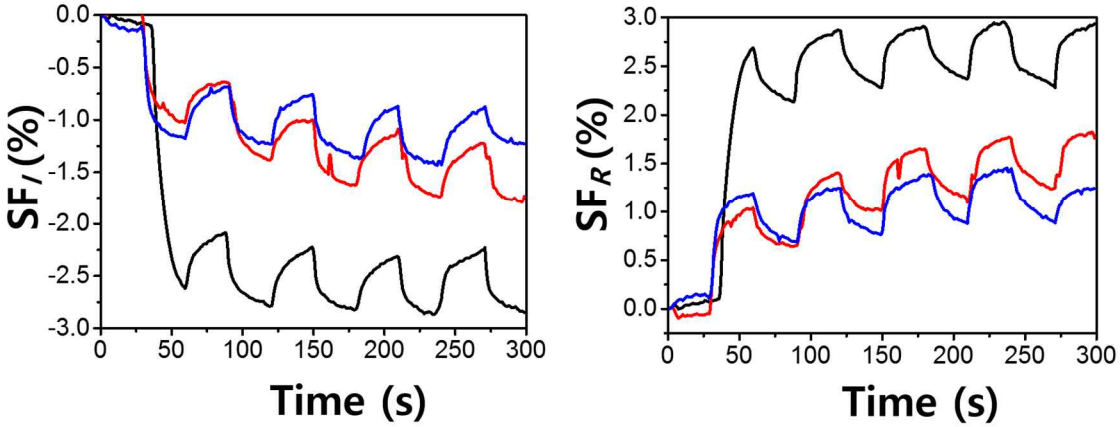

Figure 2.9. (a) Real-time current response of stretchable gas sensors at fixed NH_3 gas concentration (2000ppm). (b) Real-time resistance response of stretchable gas sensors at fixed NH_3 gas concentration (2000ppm).

2.4. Conclusion

In conclusion, we demonstrated stretchable gas sensor using nano-patterned TiO_2 coated on Au nanosheet. The gas sensor is that detect the selective gas through variation of current flow. Therefore, it should consist of active layer that response to presence of gas, and electrode layer. In here, nano-patterned TiO_2 was used as active material, and Au nanosheet and elastomer SBS block copolymer film was used as stretchable electrode. We easily synthesized nano-patterned TiO_2 for active material through block copolymer self-assembly and solvent vapor annealing process to increase the gas sensitive-area. The Au nanosheet with SBS block copolymer thin film was given stretchability to gas sensor. Also, bio-comparable TiO_2 and Au nanosheet can be applied wearable devices. Finally, we confirmed real-time current response of stretchable gas sensors at fixed NH_3 gas concentration (2000 ppm). Therefore, it has been confirmed that the stretchable gas sensor has sensing ability for selective gas.

References

1. Rao, C. N. R.; Sood, A. K.; Subrahmanyam, K. S.; Govindaraj, A., *Angew. Chem. Int. Ed*. **2009**, *48*, 7752-7777.
2. Moon, G. D.; Lim, G.; Song, J. H.; Shin, M.; Yu, T.; Lim, B.; Jeong, U. *Adv. Mater.* **2013**, *25*, 2707–2712.
3. Wang, C.; Yin, L.; Zhang, L.; Xiang, D.; Gao, R., *Sensors **2010**, 10*, 2088-21.
4. Kim, H.; Hong, M. H.; Jang, H. W.; Yoon, S. J.; Park, H. H., *Thin Solid Films* **2013**, *529*, 89-93.
5. Wang, B.; Zhao, Y.; Hu, L.; Cao, J.; Gao, F.; Liu, Y.; Wang, L., *Chin. Sci. Bull*. **2010**, *55*, 228-232.
6. Wunderlich, W.; Oekermann, T.; Miao, L.J., *Ceram. Process. Res.* **2004**, *5*, 343-354.
7. Linsebigler, A. L.; Lu, G.; Yates, J. T., *Chem. Rev.* **1995**, *95*, 735-758.
8. Hashimoto, K.; Irie, H.; Fujishima, A., *Jpn. J. Appl. Phys.* **2005**, *44*, 8269-8285
9. Ruiz, A. M.; Sakaib, G.; Corneta, A.; Shimanoeb, K.; Morantea, J.R.; Yamazoeb, N., *Sens. Actuators. B, Chem.* **2003**, *93*, 509-518.
10. Chemseddine, A.; Moritz, T., *Eur. J. Inorg. Chem.* **1999**, 235-245. volume
11. Sugimoto, T.; Okada, K.; Itoh, H. J., *Colloid Interface Sci.* **1997**, *193*, 140-143.
12. Lei, Y.; Zhang, L. D.; Fan, J. C., *Chem. Phys. Lett.* **2001**, *338*, 231-236.
13. Liu, S.; Huang, K., *Sol. Energy Mater. Sol. Cells* **2004**, *85*, 125-131.
14. Hong, S. S.; Lee, M. S.; Park, S. S.; Lee, G. D., *Catal. Today* **2003**, *87*, 99-105.
15. Seifried, S.; Winterer, M.; Hahn, H., *Chem. Vap. Deposition* **2000**, *6*, 239-244.
16. Pradhan, S. K.; Reucroft, P. J.; Yang, F.; Dozier, A. J., *Cryst. Growth* **2003**, *256*, 83-88.
17. Wu, J. M.; Shih, H. C.; Wu, W. T., *Chem. Phys. Lett.* **2005**, *413*, 490-494.
18. Wu, J. M.; Shih, H. C.; Wu, W. T.; Tseng, Y. K.; Chen, I. C., *J. Cryst. Growth* **2005**, *281*, 384-390.
19. Peng, X.; Chen, A., *J. Mater. Chem.* **2004**, *14*, 2542-2548.
20. Armstrong, A. R.; Armstrong, G.; Canales, J.; García. R.; Bruce, P. G., *Adv. Mater.* **2005**, *7*, 862-865.
21. Liu, B.; Aydil, E. S., *J. Am. Chem. Soc.* **2009**, *131*, 3985-3990.
22. Qiu, J.; Yu, W.; Gao, X.; Li, X. M., *Nanotechnology* **2006**, *17*, 4695.
23. Macak, J. M.; Tsuchiya, H.; Ghicov, A.; Yasuda, K.; Hahn, R.; Bauer, S.; Schmuki, P., *Curr. Opin. Solid State Mater. Sci.* **2007**, *11*, 3-18.
24. Shi, J.; Hara, Y.; Sun, C.; Anderson, M. A.; Wang, X., *Nano Lett.* **2011**, *11*, 3413-3419.

25. Liu, B.; Aydil, E. S., *J. Am. Chem. Soc.* **2009**, *131*, 3985-3990.

26. Yang, H. G.; Liu, G.; Qiao, S. Z.; Sun, C. H.; Jin, Y. G.; Smith, S. C.; Zou, J.; Cheng, H. M.; Lu, G. Q., *J. Am. Chem. Soc.* **2009**, *131*, 4078-4083.

27. Göpel, W.; Schierbaum, K. D., *Sens. Actuators. B, Chem.* **1995**, *26*, 1-12.

28. Bai, J.; Zhou, B., *Chem. Rev.* **2014**, *114*, 10131−10176.